Phanerozoic marine inundation of continents driven by dynamic topography above subducting slabs

Michael Gurnis

Department of Geological Sciences, University of Michigan, Ann Arbor, Michigan 48109-1063, USA

A spherical model of mantle flow constrained by the locations of trenches can be used to predict the dynamic topography of the Earth's surface, and hence the marine inundation of continents. For past periods of high sea level, the predicted geographical pattern of flooding correlates well with the geological record. The high spatial correlation may result from increased plate velocities at these times, leading to increased rates of subduction, subsidence and inundation at convergent margins.

THE fraction of continental platforms and margins inundated by shallow marine seas was high during the early to middle Palaeozoic era, low during the late Palaeozoic to early Mesozoic, when the Pangea supercontinent was assembled, and high again during the late Mesozoic to early Cenozoic[1,2]. This double-peaked inundation curve (Fig. 1*a*) is the first-order characteristic of Phanerozoic stratigraphy, and is often interpreted, first, as a eustatic (globally uniform) variation and, second, in terms of fluctuations in the age distribution of oceanic lithosphere. This latter model is supported by an empirical correlation between the Cenozoic evolution of oceanic lithosphere and the 'averaged' amount of continental flooding[3,4]. Although the average age of oceanic lithosphere can be changed by varying either ridge spreading rate or ridge length, Kominz[4] argued that it was a decrease in spreading rate which was primarily responsible for the sea-level fall since the Cretaceous period.

Besides changes in spreading rate, there may also be three other mantle convection controls on sea-level change: the characteristics of subduction[5,6], the motion of continents with respect to a large-scale pattern of dynamic topography[7,8], and changes in dynamic topography caused by supercontinent insulation[9]. Observationally, eustatic fluctuations are not the only mode of sea-level change: late Mesozoic and Cenozoic flooding-hypsometry data demonstrate that as much marine inundation resulted from regional epeirogenic as from eustatic variations[10]. A likely explanation of the eustatic and epeirogenic partitioning may rest with a detailed understanding of the implications of increased and decreased plate velocities from mantle convection models[6]. Convection models show that when plate velocities (and hence seafloor spreading rates) increase, relative sea level rises significantly faster in the vicinity of converging margins compared to the prediction for simple ridge spreading because of the additive effects of a rising eustatic sea level and subsidence of the overriding plate[6]. Bond[11] has argued that during the Cretaceous period, when spreading rates were higher[3,4], the most extensive areas of marine inundation were associated with converging margins (the western interior of North America, northern Africa and the southern part of the European platform) as predicted by the convection models. Moreover, modelled regional epeirogenic and eustatic sea-level changes are the same amplitude (a few hundred metres[6]), and consistent with observations[10].

Convection calculations offer testable predictions for models of spreading-rate-induced sea-level change. When spreading rates increase, sea level will rise eustatically, but the effect will be most pronounced at convergent margins. On the other hand, when spreading (and hence subduction) rates decrease, convergent margins will be uplifted. This implies that shallow seas would not inundate converging margins, especially if the margins were close to sea level before the period of reduced ridge spreading. If high spreading rates caused early to middle Palaeozoic inundation, the location of marine sediments should correlate with the position of subduction-induced dynamic topography, as it is these areas of continent which would have been subsiding. The same should hold true for the period of high sea level in the late Jurassic to early Cretaceous. If the fall in sea level during the late Palaeozoic to early Mesozoic was caused by a decrease in ridge spreading, then marginal marine sediments should be rare or absent in areas of depressed dynamic topography, as it is these continental areas which we expect to be uplifting.

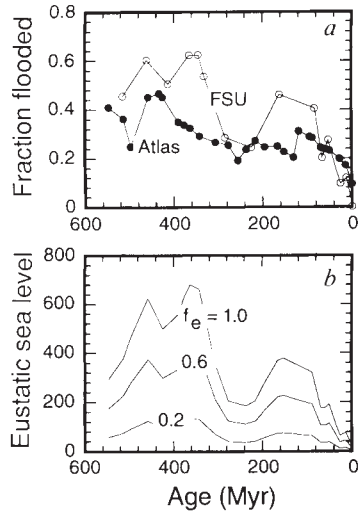

FIG. 1 *a*, Fraction of continent flooded as a function of geologic age inferred from the *Paleomap Paleogeographic Atlas*[13] and the lands of the former Soviet Union[17] (FSU). *b*, Eustatic sea levels (e_R), inferred to be fractions (f_e) of the sea level required to inundate the FSU shown in *a*, assuming an average continental hypsometry.

In order to predict subduction-induced dynamic topography over the Phanerozoic, the history of spreading and subduction, including the position of subduction (trenches) and subduction rates need to be incorporated into a dynamic sea-level model. Recently, the relationship between Cenozoic subduction and three-dimensional seismic heterogeneity in the mantle has been studied by introducing 'slablets' into the mantle, constrained by the location of Cenozoic subduction[12]. A high correlation was

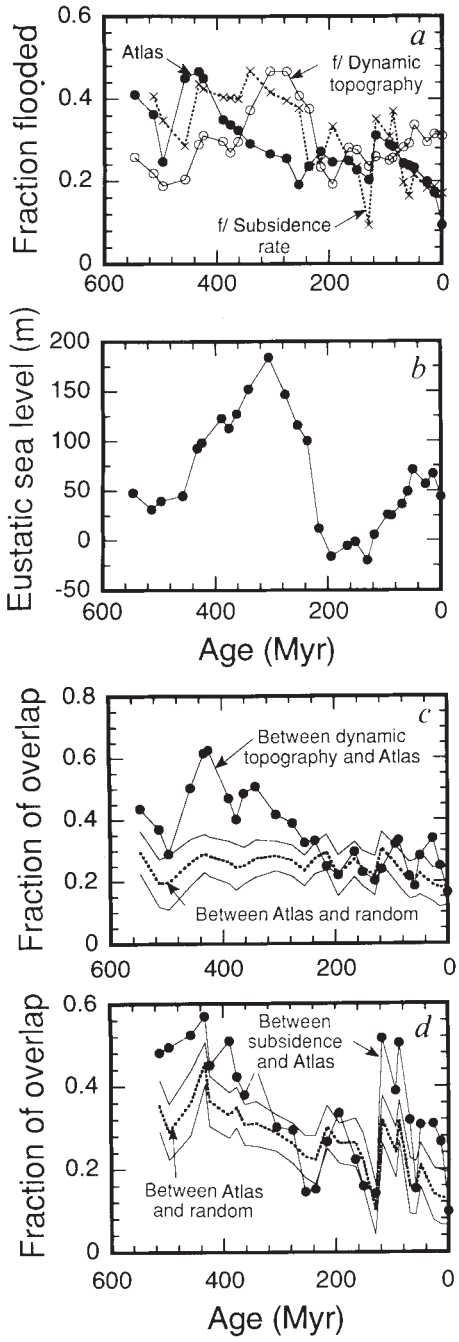

FIG. 2 Predictions from a spherical model of whole mantle flow assuming a constant ridge spreading rate. *a*, Flooding predicted from the dynamic topography and the time-derivative of dynamic topography (subsidence rate) compared to inundation shown in the *Atlas*[13]. *b*, Eustatic sea level (e_D) predicted from the dynamic topography. *c*, Fraction of overlap between flooding predicted from dynamic topography and the *Atlas*. *d*, Fraction of overlap between the flooding predicted from subsidence rate and the *Atlas*. In *c* and *d*, the dotted line is the mean overlap between the *Atlas* and 100 randomly generated models, with 99% confidence limits shown as surrounding solid lines.

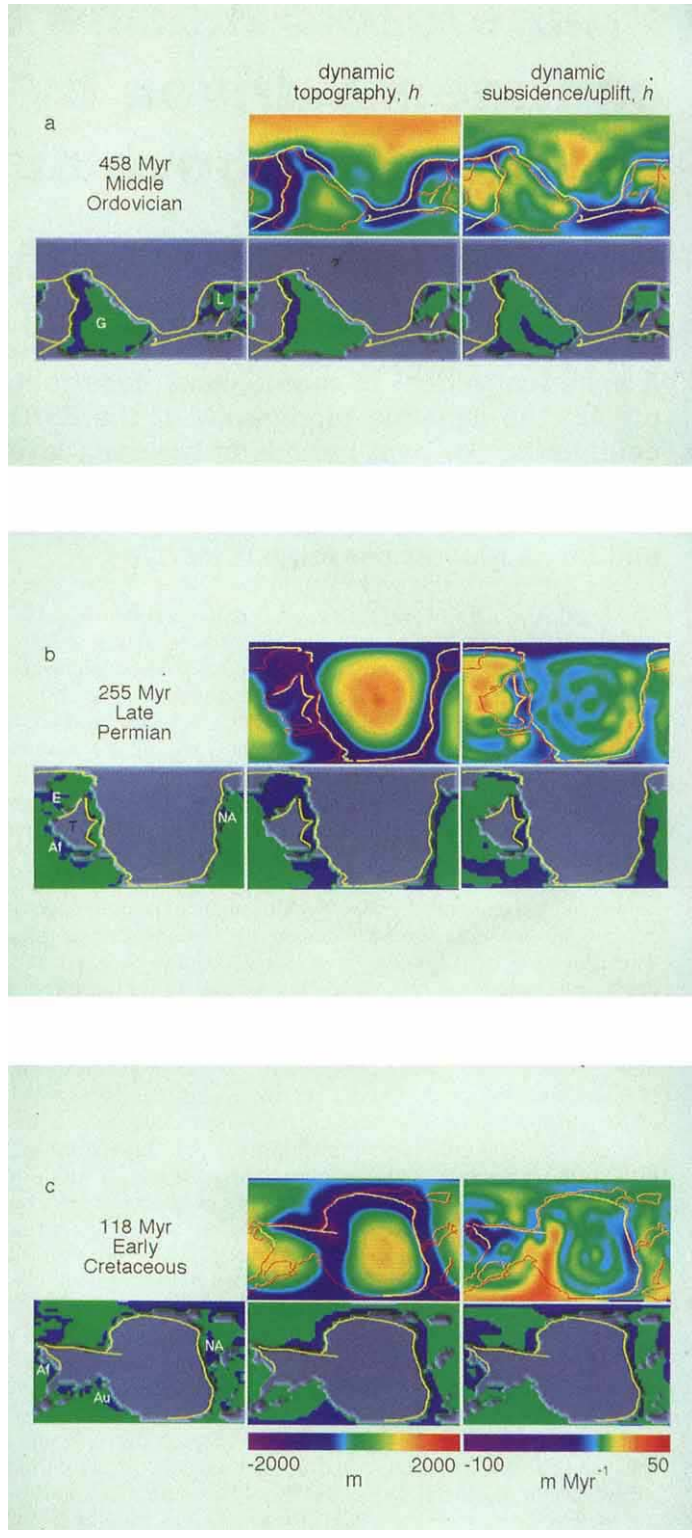

FIG. 3 Continental inundation (dark blue) from the *Paleomap Paleogeographic Atlas*[13] (far left) compared to predicted flooding from dynamic topography (centre column) and from subsidence rate (far right) during the middle Ordovician (*a*), late Permian (*b*) and early Cretaceous (*c*). Also shown for each time interval is the actural dynamic topography and the time derivative of dynamic topography with colour shading as follows. Trenches are shown as yellow lines and continents by red lines; the continent function is the sum of dark blue and green areas (also shown as positive relief). In *a*, G is Gondwana and L is Laurentia; *b*, T is Tethys, Af is Africa, E is Europe and NA is North America; and in *c*, Au is Australia, Af is Africa and NA is North America.

found between predicted areas of cold mantle and observed seismic structure, suggesting that mantle flow models constrained by palaeo-trench locations can be used to understand sea-level changes and continental epeirogeny. Although the positions of converging margins with respect to continents are known to varying degrees of reliability through the Phanerozoic, oceanic lithosphere from the late Mesozoic and older is not preserved, and the history of spreading and subduction rate cannot be directly constrained. Given this ambiguity, one approach is to

assume a constant spreading rate and a constant age of lithosphere subducting over the Phanerozoic. An alternative approach is to constrain spreading and subduction rates from eustatic sea level; eustasy is obtained from the fractional inundation of a continent.

Predicting inundation in a spherical flow model

The *Paleomap Paleographic Atlas* (ref. 13), hereafter referred to as the *Atlas*, synthesizes the following Phanerozoic data: (1) continental outlines and positions, (2) areas of exposed continent, (3) areas of continent inundated by shallow seas, and (4) the position of oceanic trenches. Oceanic trench positions constrain where oceanic lithosphere sinks into the mantle.

The integrated flux of material subducted into the mantle forms a three-dimensional function of mantle density anomalies, $S(t,\theta,\phi,r)$, where t is time, θ and ϕ are latitude and longitude, and r is radius. S is convolved with dynamic response functions in the Fourier domain to predict dynamic topography, $h(t,\theta,\phi)$, on the surface of the sphere[14]. As dynamic topography is computed as a function of time, differentiation of h gives uplift and subsidence of the surface of the sphere, $dh(t,\theta,\phi)/dt$. In conjunction with the 'continent function', $C(t,\theta,\phi)$ (here defined as a map set to unity where there is continent, either flooded or exposed, and zero where there is no continent), the positions of dynamically depressed or actively subsidising continental regions can be computed. (With the simplified Green's function technique[14] used, the position of continents does not affect mantle flow.) With appropriate critical values, h_c or $\dot{h}_c$ as given below, these two functions give the predicted positions of shallow continental seas, $F(t,\theta,\phi)$. Specifically, using reconstructed h and $\dot{h}$, F is set to unity where $hC < e_T + h_c$ (where e_T is the total eustatic sea level, see below) or $\dot{h}C < \dot{h}_c$ and is set to zero elsewhere. This simple prediction of pattern is the prudent approach because the *Atlas*[13] only contains the extent of inundation and not the three-dimensional magnitude of inundation which might eventually be constrained with isopachs of sedimentary units. Clearly, a more realistic model would combine e_T, h, and $\dot{h}$, perhaps linearly, because shallow marine sediment will only accumulate in areas which are both dynamically depressed below sea level and subsiding. The effect of the geoid on regional variations in sea level is ignored. Continental flooding is a function of both dynamic topography and the geoid[8], but because admittance (ratio of geoid to dynamic topography) is small (less than 0.1) for long wavelengths[14], the effect of dynamic topography is significantly more important than the geoid.

There are two contributions to the total eustatic sea level, e_T: the dynamic topography, e_D, and the ridge, e_R, components. The dynamic topography component is just the average height of the topography in the oceanic regions generated by mantle flow[8]. The ridge component is inferred to be a fraction of the sea-level rise required to flood the Russian platform assuming an averaged continental hypsometric curve[15]. This region has experienced little Mesozoic and Cenozoic tectonic disturbance and may constrain eustatic sea-level change[16]. The Phanerozoic inundation curve of the lands of the former Soviet Union[17] is used (Fig. 1*a*). A fraction, f_c, of this regional sea level is assumed to be eustatic and three values (0.2, 0.6 and 1) are used in the calculations described below and shown in Fig. 1*b*. It must be emphasized that if hypothesized mantle convection controls on sea level are important, then any single continental region is unlikely to constrain eustatic sea level over a time as long as the Phanerozoic.

In the model, material is injected vertically into a spherical shell at either a constant rate and age (that is, the age of the oceanic lithosphere just before subduction, τ_s) or at an increasing rate and decreasing age when e_R increases. As dynamic depression of the surface above a slab occurs over a few thousand kilometres[18], the neglect of both slab dip and the elastic rigidity of the lithosphere are reasonable assumptions[19]. The relations between spreading rate, age of lithosphere (τ_s) and eustatic sea level (e_R) are well known[20]. The velocity of descent through the upper mantle is assumed to be equal to the spreading rate and is either constant or obtained from e_R. In a layered convection model, material disappears when it reaches 670 km depth because dynamic topography vanishes when slabs become compensated on an internal boundary[14]. In the case of whole-mantle convection, slab buoyancy continues through 670 km depth, but potentially at a slower rate because of greater viscosity in the lower mantle[21].

Three quantities, in addition to h and $\dot{h}$, are extracted as a function of time: the predicted amount of total inundation; maps showing predicted shallow seas; and the overlap between positions of observed (F_o) and predicted (F) shallow seas. For each geologic age for which there is a map in the *Atlas*, the overlap between observed and inferred inundation is determined. Overlap between two maps is normalized by mean flooding between the *Atlas* and dynamic model. Moreover, overlaps are found between the *Atlas* and a suite of models with random distributions of marine deposits assuming the same amount of inundation predicted by the dynamic model. Comparing the overlap between *Atlas* and dynamic models with the overlap between *Atlas* and random models eliminates the bias introduced by the dependence of overlap on F and C.

Predictions of Phanerozoic inundation

A variety of models with buoyancy constrained by trench locations were explored. For a given mantle model (primary parameters are whole-mantle versus layered-mantle convection, rheological stratification, and a history of ridge spreading rate) a number of continental flooding histories were run with h_c and $\dot{h}_c$ systematically varied until an average flooding of 0.3 (the observed value) was obtained. Figure 2*a* shows the fraction of marine inundation over the Phanerozoic for a model with whole-mantle flow and a radial stratification in viscosity. For this particular model, τ_s is 100 Myr, h_c is -500 m and $\dot{h}_c$ is -1 m Myr^{-1}; these values are assumed constant through the Phanerozoic. The viscosity distribution is identical to model W4a from Hager and Clayton[22]: a moderately high viscosity lithosphere with a factor of 30 change in viscosity at 670 km depth. The spreading rate and rate of descent of cold material in the upper mantle are assumed to be 5 cm yr^{-1}, decreasing to 2 cm yr^{-1} below 670 km (roughly consistent with convection in a fluid with depth-dependent viscosity[23]).

When spreading rates are constant, and for both whole-mantle and layered-mantle convection models, the general pattern of fractional inundation (more flooding in the Palaeozoic, less flooding in the early Mesozoic, and more flooding again in the late Mesozoic and early Cenozoic) is not reproduced (Fig. 2*a*). Indeed, the greatest predicted inundation occurs when observed inundation is near a minimum. The pulse in h-controlled flooding during the late Palaeozoic to early Mesozoic is caused both by the long-term stability of trenches around the margin of Pangea and by the tangle of trenches close to the Tethys sea (Fig. 3*b*). Because the spreading rate is held constant, the only control on eustasy is dynamic topography in the oceanic regions (Fig. 2*b*). Modelled eustasy undergoes a long-term $\sim$200-m change driven by trench rearrangement. High eustatic sea level is caused by long-term stability of trenches around Pangea. The peak in eustatic sea level correlates with the peak in h-controlled flooding, but it is the dynamic depression of the margins of Pangea, not the long-wavelength pushing up of the oceanic regions, which primarily controls the peak in inundation.

A different view of sea-level change emerges from the location of inundation. Maps of continental positions, flooding and trenches (taken from the *Atlas*[13]) are shown in Fig. 3, where they are compared with dynamic topography, the rate of change of dynamic topography, and flooding predicted from h and $\dot{h}$. These comparisons are performed at three different ages: middle Ordovician, 458 Myr ago (Fig. 3*a*), late Permian, 255 Myr ago (Fig. 3*b*) and early Cretaceous, 188 Myr ago (Fig. 3*c*).

During the Middle Ordovician the contininents are dispersed and nearly at peak marine inundation. North America or Laurentia ('L' in Fig. 3*a*) and the margin of the large Gondwana continent ('G') are the principle areas of flooding. Regionally persistent subduction to the west of Gondwana and to the north and west of Laurentia give rise to the h-predicted flooding on the western margin of Gondwana and what is now the western margin of North America, respectively. The *Atlas*[13] shows subduction appearing to the south of Laurentia (now the eastern seaboard of North America) in the Early Ordovician, and this leads to subsidence to the south of Laurentia persisting to Middle Ordovician (Fig. 3*a*), and ultimately leads to the $\dot{h}$-predicted flooding in Laurentia. The inferred pattern of inundation is extremely well predicted by models based on h and, to a lesser extent, on $\dot{h}$ (Fig. 3*a*). Similar correlations can be found for other early to middle Palaeozoic times and for other models including those with layered convection. The correlation between observed and predicted inundation is highly significant (Fig. 2*c*). Through the entire Palaeozoic era, overlap is significantly greater than the 99% confidence interval of expected overlap between *Atlas* and random models. There is also significant overlap between $\dot{h}$-flooding and the *Atlas* for early and middle Palaeozoic, well above the 99% confidence interval of overlap betwen the *Atlas* and random models (Fig. 2*d*).

By early Carboniferous time, Pangea is nearly assembled and surrounded by converging margins. A stationary configuration of continents and margins up to the late Permian leads to a simple degree two pattern of dynamic topography (Fig. 3*b*). Such topography bows a considerable portion of continental margins downward (Fig. 3*b*) leading to a near maximum in the predicted fraction of inundation ($\sim$0.5, Fig. 2*a*). During the late Permian (Fig. 3*b*) most inundation occurred in northern Africa (shown as Af) and Europe (E), which form the areas south and north of the Tethys sea (T). At this time, flooding does not occur in areas near trenches or areas predicted to be flooded. Significant amounts of flooding are predicted on the western margins of the Americas where there is no evidence of flooding in the *Atlas*[13]. Also, subsidence and flooding are predicted around the margins of Pangea, as the whole of Pangea moves with its attendant margins. Such extensive inundation in areas predicted by these models, especially by h, did not occur (Fig. 3*b*). Although poor correlations occur in the entire late Palaeozoic to early Mesozoic interval, the complete avoidance of margin flooding is not as clear as it is at this late Permian time. Quantitatively, overlaps between h- and $\dot{h}$-flooding and the *Atlas* are indistinguishable from overlap between random models and the *Atlas*. During the Permian, the overlap between $\dot{h}$-predicted flooding and the *Atlas* is less than the overlap of *Atlas* and random models at greater than the 99% confidence level (Fig. 2*d*), suggesting the nearly complete avoidance of flooding on converging margins.

By Jurassic time the Pangea supercontinent started to break up, but even as late as early Cretaceous time, the simple degree two pattern in dynamic topography persists (Fig. 3*c*). Indeed, the strong degree two pattern evident in the present day geoid and seismic tomography may be partly controlled by this Mesozoic arrangement of trenches[12,24,25]. A strong circum-Pacific pattern of inundation is predicted from this dynamic topography, as North and South America move westward over the previous positions of subduction. There is also some inundation predicted from $\dot{h}$. There was significant flooding in western North America, northern Africa and Australia. Correlations based on both h and $\dot{h}$ (Fig. 3*c*) predict North American and north African flooding well, but not that in Australia. The *Atlas*[13] has, however, omitted a highly probable palaeo-trench to the northeast of Australia during the Jurassic and Cretaceous[26] period. The overlap between h-predicted flooding and the *Atlas* is not as significant as during the Palaeozoic (although still statistically significant) (Fig. 2*c*). The overlap with $\dot{h}$-predicted flooding and the *Atlas* is particularly high during the Cretaceous period (Fig. 2*d*).

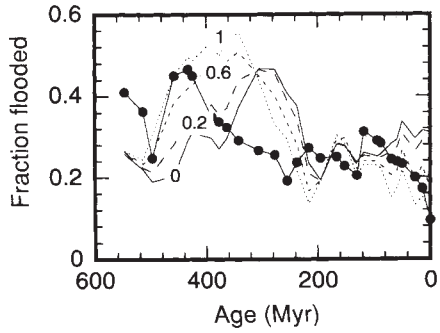

FIG. 4 Fraction of continents flooded for a series of four models with spreading rates constrained by eustatic sea levels (shown in Fig. 1*b*). The values labelling the curves are f_e. The case with $f_e = 0$ has spreading rate constant as a function of time. For each model, the values of h_c and $\dot{h}_c$ are: -500 m and -1 m Myr^{-1} for $f_e = 0$; -580 m and -1 m Myr^{-1} for 0.2; -760 m and -1.3 m Myr^{-1} for $f_e = 0.6$; and -936 m and -2 m Myr^{-1} for $f_e = 1$.

In order to resolve the discrepancy between observed and predicted inundation (Fig. 2*a*), exemplified by the peak in h-predicted flooding during the late Palaeozoic, a series of models were calculated with variations in ridge spreading rate, and hence subduction rate, constrained by eustatic sea levels (Fig. 1*b*); spreading rates can reach values of 11 cm yr^{-1} in the Palaeozoic when $f_e = 1.0$. Flooding for four values of f_e shows that the peak in inundation predicted by models is only slightly lowered in amplitude and shifted earlier to the middle Palaeozoic (Fig. 4). Constraining eustatic sea level with the average inundation of the *Atlas* (Fig. 1*a*), instead of Russian platform inundation, also fails to remove the late Palaeozoic peak in modelled flooding. Upper-mantle models, with f_e larger than zero, fare even less well compared to the whole-mantle models presented. Clearly, plausible variations in spreading rate constrained by eustatic variations are unable to lead to relatively low dynamic topography around the margins of Pangea during late Palaeozoic and early Mesozoic. Importantly, for a range of models with various eustatic and subduction rate histories, the pattern of overlap between modelled flooding and the flooding shown in the *Atlas* (so clearly evident in Fig. 2*c* and *d*) changes by only a minor amount. Overlap is relatively insensitive to both eustatic fluctuations and subduction rate.

Implications and limitations

The results obtained here by meshing a palaeogeographic atlas[13] with a spherical mantle flow model corroborate the hypothesis advanced from studies of convection dynamics with plates, that inundation should be localized in the vicinity of ocean–continent converging margins when sea levels are high[6]. The mechanism may be simple: when spreading rates increase, rates of subduction and hence subsidence of converging margins also increase, giving rise to both high eustatic sea levels and regional localization of inundation at converging margins. But a major discrepancy is evident in the extensive flooding of margins around Pangea, caused by a modelled stable configuration of convergence during the late Palaeozoic and early Mesozoic, when sea levels were low. This extensive flooding is insensitive to large modelled drops in eustatic sea level and spreading and subduction rates at the end of the Palaeozoic.

Why are fractional inundation and, apparently, eustatic sea level so low at a time when inundation is predicted to be so high by the flow model? Three possibilities are considered: supercontinent insulation, a change in the ocean water mass, and unaccounted-for convergent margins in the ocean around Pangea. Thermal insulation, leading to uplift during periods of stability, may occur under supercontinents[27,28] but is not present in the model because the energy equation has not been solved. Augmented dynamic topography is expected to have the largest effect within the interior of Pangea away from converging margins[9],

and the addition of the effect is unlikely to cause exposure of converging margins. Second, if the mass of ocean water significantly decreased at the end of the Palaeozoic, then the margins might become exposed. Sea level, however, would have to be lowered by more than 1 km (Fig. 3*b*) in order to counteract the depressed converging margins; this change is an order of magnitude larger than the fluctuations during the most recent glacial epochs[29]. Moreover, this effect fails to account for the lack of inundation of convergent margins. A final possibility is the presence of subduction zones, like Marianas and Tonga, entirely within the ocean surrounding Pangea. If spreading rate were constant, while additional convergent and divergent margins within the ocean formed, the average age of oceanic lithosphere would decrease and lead to uplift above the convergent continental margins[30]. A decreased average age of ocean floor would normally lead to increased eustatic sea level, but subduction zones within oceans would counteract this effect by decreasing the overall dynamic topography within oceans[5]. This final model is preferred, because it also leads to active uplift of Pangea's active margins which apparently were not flooded at this time (Fig. 3*b*).

The models can be made more realistic, and can be tested with detailed observations. The details of regional subsidence predicted by global flow models can be compared with tectonic subsidence curves (derived from single boreholes corrected for sediment loading and compaction[31]) and against regional tilting events[19]. The flow models also predict extensive and rapid regional uplift, which can in principle be related to regional unconformities[32]. The models can be improved by using (1) the coupled solution of the energy and momentum equation and tectonic plates, (2) more realistic inundation models with sediment involving both h and $\dot{h}$, and (3) tracking fixed points on continental plates which move with respect to the mantle. It appears that we are on the verge of a new understanding of the underlying mantle dynamics driving global stratigraphic architecture. □

Received 16 November 1992; accepted 9 June 1993.

1. Hallam, A. *A. Rev. Earth planet. Sci.* **12,** 205–243 (1984).
2. Wise, D. U. in *The Geology of Continental Margins* (eds Burk, C. A. & Drake, C. L.) 45–58 (Springer, New York, 1974).
3. Hays, J. D. & Pitman, W. C. *Nature* **246,** 18–22 (1973).
4. Kominz, M. A. *Am. Assoc. Petrol. Geol. Mem.* **36,** 109–129 (1984).
5. Hager, B. H. (abstract) *EOS* **61,** 374 (1980).
6. Gurnis, M. *Science* **250,** 970–972 (1990).
7. Hager, B. H., Clayton, R. W., Richards, M. A., Cromer, R. P. & Dziewonski, A. M. *Nature* **313,** 541–545 (1985).
8. Gurnis, M. *Nature* **344,** 754–756 (1990).
9. Gurnis, M. *Geophys. Res. Lett.* **17,** 623–626 (1990).
10. Bond, G. *Geology* 247–250 (1978).
11. Bond, G. C. *Tectonophysics* **61,** 285–305 (1979).
12. Richards, M. A. & Engebretson, D. C. *Nature* **355,** 437–440 (1992).
13. Scotese, C. R. & Golonka, J. *PALEOMAP Paleogeographic Atlas*, PALEOMAP Progress Report 20 (Dept of Geol., Univ. of Texas, Arlington, 1992).
14. Richards, M. A. & Hager, B. H. *J. Geophys. Res.* **89,** 5987–6002 (1984).
15. Gurnis, M. *Geology* **21,** 29–32 (1883).
16. Sahagian, D. L. & Holland, S. M. *Geology* **19,** 1209–1212 (1991).
17. Hallam, A. *Nature* **269,** 769–772 (1977).
18. Hager, B. H. *J. geophys. Res.* **89,** 6003–6015 (1984).
19. Mitrovica, J. X., Beaumont, C. & Jarvis, G. T. *Tectonics* **8,** 1079–1094 (1989).
20. Turcotte, D. L. & Schubert, G. *Geodynamics* (Wiley, New York, 1982).
21. Richards, M. A., Ricard, Y., Lithgow-Bertelini, C. & Engebretson, D. C. (abstract) *EOS Spring Meeting Supplement* 280 (1992).
22. Hager, B. H. & Clayton, R. W. in *Mantle Convection* (ed. Peltier, R. W.) 657–763 (Gordon & Breach, New York, 1989).
23. Gurnis, M. & Davies, G. F. *Geophys. J. R. astr. Soc.* **85,** 523–541 (1986).
24. Chase, C. G. & Sprowl, D. R. *Earth planet. Sci. Lett.* **62,** 314–320 (1983).
25. Davies, G. F. *Earth planet. Sci. Lett.* **69,** 187–192 (1984).
26. Veevers, J. J. *Phanerozoic Earth History of Australia* (Clarendon, Oxford, 1984).
27. Anderson, D. L. *Nature* **297,** 391–393 (1982).
28. Gurnis, M. *Nature* **332,** 695–699 (1988).
29. Hallam, A. *Phanerozoic Sea-Level Changes* (Columbia Univ. Press, New York, 1992).
30. Gurnis, M. *Science* **255,** 1556–1558 (1992).
31. Kominz, M. A. & Bond, G. C. *Geology* **19,** 56–60 (1991).
32. Sloss, L. L. *Bull. geol. Soc. Am.* **74,** 93–114 (1963).

ACKNOWLEDGEMENTS. I thank M. Richards for his dynamic response function software, H. Pollack for his spherical harmonic analysis software, and B. Hager, H. Pollack, R. Van der Voo and B. Wilkinson for comments. L Ruff suggested the overlap statistic. This research has been supported by the National Science Foundation, the David and Lucile Packard Foundation and the Petroleum Research Fund.

Crystal structure of bacteriophage T7 RNA polymerase at 3.3 Å resolution

Rui Sousa*, Yong Je Chung†, John P. Rose*† & Bi-Cheng Wang*†‡

Departments of * Biological Sciences and † Crystallography, University of Pittsburgh, Pittsburgh, Pennsylvania 15260, USA

The crystal structure of T7 RNA polymerase reveals a molecule organized around a cleft that can accommodate a double-stranded DNA template. A portion (~45%) of the molecule displays extensive structural homology to the polymerase domain of Klenow fragment and more limited homology to the human immunodeficiency virus HIV-1 reverse transcriptase. A comparison of the structures and sequences of these polymerases identifies structural elements that may be responsible for discriminating between ribonucleotide and deoxyribonucleotide substrates, and RNA and DNA templates. The relative locations of the catalytic site and a specific promoter recognition residue allow the orientation of the polymerase on the template to be defined.

CELLULAR and chloroplast RNA polymerases are large multisubunit enzymes. RNA polymerase (RNAP) from *Escherichia coli*, for example, is an enzyme of M_r 500K that contains five subunits of four different types[1]. The large size and complexity of these RNAPs has made structural studies difficult. Mitochondria and many bacteriophages encode smaller single-subunit RNAPs[2–7]. Bacteriophage T7 RNAP executes promoter-specific transcription *in vivo* and *in vitro* as a 99K single-subunit enzyme[8] and was the first of this family of structurally simple RNAPs to be identified[9] and overexpressed[8]. For these reasons, T7 RNAP is an attractive RNAP for structural studies. The mechanism of T7 RNAP transcription shares some apparent similarities to that of the multisubunit RNAPs. Like *E. coli* RNAP, T7 RNAP recognizes a specific promoter sequence[10], unwinds the double-stranded DNA to expose the coding strand for templating[11], initiates *de novo* preferentially with a purine, goes through an initial 'abortive' phase of transcription (during which short (2–9 base) transcripts are synthesized and released from the ternary

‡ To whom correspondence should be addressed.